Analysis of Directive Radiation From a Line Source in a Metamaterial Slab With Low Permittivity

Giampiero Lovat, *Member, IEEE*, Paolo Burghignoli, *Member, IEEE*, Filippo Capolino, *Senior Member, IEEE*, David R. Jackson, *Fellow, IEEE*, and Donald R. Wilton, *Fellow, IEEE*

***Abstract*—In this paper an investigation is presented of metamaterial structures excited by a line source aimed at producing narrow directive beams. The structure under consideration is a grounded slab made of a homogeneous metamaterial medium with a plasma-like dispersive permittivity; for low values of the slab permittivity an extremely directive beam pointing at broadside can be obtained. Conditions for the maximization of radiation at broadside are given and the narrow-beam effect is shown to be related to the excitation of a leaky mode supported by the slab, with radiation maximization corresponding to small and equal values of the phase and attenuation constants. The frequency bandwidth and directivity are expressed in a simple closed form in terms of the attenuation constant of the leaky mode. By increasing the slab height for a fixed frequency, the leaky mode is analytically shown to give rise to a beam that is scanned from broadside to the critical angle for plane-wave refraction, thus being confined to a narrow angular region around broadside. Numerical results are given that illustrate these features, and full-wave simulations of a metamaterial structure made of an array of metallic cylinders are presented that confirm the results of the analytical study. The case of a line source inside a semi-infinite metamaterial region is also considered and its radiation characteristics compared with those of the metamaterial slab.**

***Index Terms*—Artificial dielectrics, broadside radiation, electromagnetic band gap, leaky waves, metamaterials, plasma.**

I. Introduction

ELECTROMAGNETIC band-gap (EBG) materials are periodic structures composed of metallic or dielectric elements embedded in a homogeneous background [1]–[5]: their main property is to inhibit propagation of electromagnetic waves in a certain frequency range, and their characteristics depend on the geometry and the periodicity of the structure. More generally, metamaterial structures are periodic structures that exhibit interesting material properties that conventional dielectric structures do not. It is known that, under suitable conditions, these structures can be homogenized when their period is much smaller than the wavelength and modeled as media with an effective permittivity and permeability, presenting some interesting features. For example, a structure composed of a periodic array of metallic cylinders and/or metallic strips with spatial period small with respect to the wavelength behaves as a homogenous material with an effective dielectric permittivity that exhibits a plasma-like behavior (see Fig. 1). The possibility of simulating such plasma behavior by means of artificial dielectrics was already established during the fifties and sixties by Brown [6], Bracewell [7], and Rotman [8]. More recently, several researchers have proposed other structures or alternative analyses in order to synthesize homogeneous materials having a dielectric permittivity and/or magnetic permeability with a frequency-dependent behavior; the main characteristic of such effective constitutive parameters is to be negative or to have a very small positive value (nearly zero) in a certain frequency range [9]–[17]. The possibility of fabricating these artificial materials has opened the way to the study and the design of several interesting devices with novel specific electromagnetic features (see, e.g., [18]–[25]).

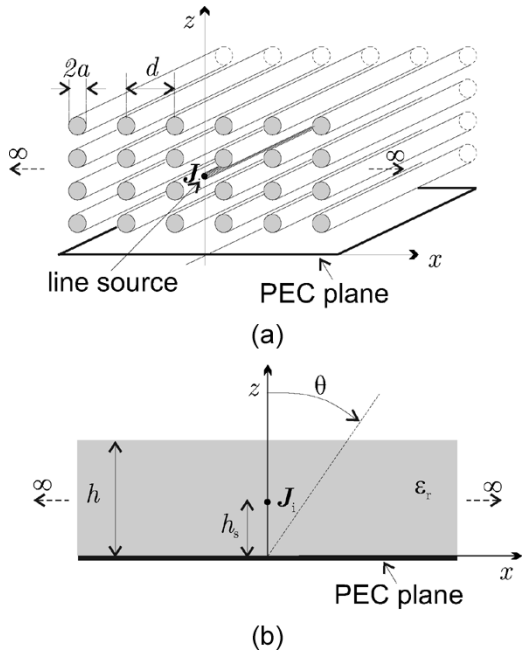

Fig. 1. (a) Example of a metamaterial structure excited by an electric line source. The structure is composed of a finite number of periodic rows of metallic cylinders with radius a and spatial period d, small with respect to the wavelength, above a perfectly-conducting ground plane. (b) Equivalent homogenized structure, modeled as a grounded plasma slab with relative permittivity ε_r.

Manuscript received April 15, 2005; revised October 10, 2005. This work was supported in part by the EU-funded project METAMORPHOSE (FP6/NMP3-CT-2004-500252) and in part by the Texas Advanced Technology Program.

G. Lovat is with the Department of Electrical Engineering, "La Sapienza" University of Rome, 00184 Rome, Italy (e-mail: lovat@die.uniroma1.it).

P. Burghignoli is with the Department of Electronic Engineering, "La Sapienza" University of Rome, 00184 Rome, Italy.

F. Capolino is with the Department of Information Engineering, University of Siena, 53100 Siena, Italy.

D. R. Jackson and D. R. Wilton are with the Department of Electrical and Computer Engineering, University of Houston, Houston, Texas 77204-4005 USA.

Digital Object Identifier 10.1109/TAP.2006.869925

The issue of enhancing the broadside directivity of a source embedded in an artificial medium has been addressed by several authors both in the optical and in the microwave ranges [26]–[34]. In particular, the use of microcavities [28], [29] or planar defects in a photonic crystal [30]–[32] to reduce the angular range of the radiated field has been illustrated.

In [26], [27], and [33], a metamaterial slab has been considered as a structure that, under suitable conditions, confines in a very narrow beam the energy radiated by a source embedded inside the metamaterial; in particular, Enoch *et al.* furnished in [33] a theoretical explanation of the directivity enhancement based on the wavenumbers of the propagating plane waves within the structure. In this work we show how the directive radiation attainable with low-permittivity homogeneous metamaterial slab structures is directly related to the excitation of a *leaky mode* with low attenuation. Properties of leaky modes in a plasma slab have already been studied in [35] and [36] and in a double-negative metamaterial grounded slab in [37]; application to frequency-scanning leaky-wave antennas was studied in [38] and [39], while the connection between leaky waves and high directivity has been suggested in [40] for a different electromagnetic band-gap structure.

It should be noted that in [37] some features of broadside radiation from leaky waves in double-negative metamaterial slabs have been described. In this work we analyze the case of an electric line source inside a grounded *positive* metamaterial slab. In addition to deriving simple design formulas to maximize the radiation at broadside (as was done in [37] for double-negative slabs), we explore the basic physical properties of such antenna structures, including directivity, pattern bandwidth, and angular limits for directive radiation. The main features of the radiated beam are expressed in terms of the wavenumber of the leaky mode, and numerical results are presented that verify the key role of leaky waves in determining the directive radiation. Moreover, results are obtained for an *actual* metamaterial structure composed of metallic cylinders to validate the theory.

After an investigation of the metamaterial plasma-slab structure, the case of a line source inside a *semi-infinite* metamaterial region is considered. This structure can also obtain highly directive patterns, although in this case the effect is not due to a leaky wave, but rather to a ray-optics effect as explained in [33]. A more detailed explanation for the effect in terms of wave phenomenology can be provided by examining the field at the interface, and it is shown that the directive pattern is due to the dominance of a lateral-wave type of field that exists on the interface. Simple formulas for the power density at broadside and the directivity are obtained for this case as well.

The paper is organized as follows. In Section II, the radiative properties of the metamaterial slab structure are investigated, and a condition is derived to obtain maximum power density radiated at broadside. An approximate closed-form expression for the relevant pattern bandwidth is then obtained. The main characteristics of the far-field pattern, including radiation off broadside, are also illustrated. In Section III, a leaky-wave explanation of the enhanced-directivity effect is provided. In particular, the condition for obtaining maximum power density radiated at broadside, the directivity at broadside, and the angular limits of the directive radiation are expressed in terms of the properties of the relevant leaky wave. The case of an electric line source radiating in a metamaterial plasma half space is then investigated in order to explore the nature of the radiation from this type of structure, and to show that the cause of the narrow-beam effect in this case is due to a lateral-wave type of field on the interface. In Section IV, an actual metamaterial slab structure composed of a periodic array of metallic cylinders is investigated by means of a full-wave numerical approach in order to validate the previous analysis. Finally, in Section V, conclusions are drawn.

II. Radiative Properties

The structure considered here is a plasma slab of height h on a perfectly conducting plane, excited by an electric line source $J_{\rm i}$ along y, embedded in the plasma medium at a distance $h_{\rm s}$ from the ground plane [see Fig. 1(b)]. For the excited polarization (TE_z, with the E field polarized along y), the plasma is modeled as lossless, homogeneous, and isotropic, with relative permeability $\mu_r = 1$ and relative permittivity

$$\varepsilon_{\rm r}(f) = 1 - \frac{f_{\rm p}^2}{f^2} \tag{1}$$

where $f_{\rm p}$ is the plasma frequency. When $f < f_{\rm p}$, the relative permittivity $\varepsilon_{\rm r}$ is negative and the plasma is said to be opaque, whereas, when $f > f_{\rm p}$, $\varepsilon_{\rm r}$ is positive and the plasma is said to be transparent: the latter is the case we are interested in, with particular reference to the frequency range in which $\varepsilon_{\rm r}$ has very low values (i.e., $\varepsilon_{\rm r} \ll 1$).

A. Maximization of the Power Density Radiated at Broadside

The electric field in the air region excited by a unit amplitude electric line source can be represented as an inverse Fourier transform,

$$E_y(x,z) = \frac{1}{2\pi}\int_{-\infty}^{+\infty} \tilde{E}_y(k_x) e^{-j(k_x x + k_{z0} z)} \mathrm{d}k_x \tag{2}$$

where $k_{z0} = \sqrt{k_0^2 - k_x^2}$ is the vertical wavenumber in air ($k_0 = 2\pi/\lambda_0$ is the free-space wavenumber) with $\Im\mathrm{m}\{k_{z0}\} \leq 0$ in order to satisfy the radiation condition at infinity, and the spectral electric field $\tilde{E}_y(k_x)$ at the air-slab interface is [41, sec. 3.9]

$$\tilde{E}_y(k_x) = -\frac{jZ_0 Z_1 \sin(k_{z1} h_{\rm s})}{Z_0 \cos(k_{z1} h) + jZ_1 \sin(k_{z1} h)}. \tag{3}$$

Here $Z_0 = \eta_0 k_0/k_{z0}$ and $Z_1 = \eta_0 k_0/k_{z1}$ are the relevant TE characteristic impedances (η_0 is the free-space characteristic impedance) and $k_{z1} = \sqrt{\varepsilon_{\rm r} k_0^2 - k_x^2}$ is the vertical wavenumber inside the slab.

The far-zone electric field can readily be obtained through an asymptotic evaluation of (2) for large distances ρ from the origin [42, Sec. 4.2]. The result is $E_y(\rho,\theta) = E_y^{\rm ff}(\theta)\, e^{-jk_0\rho}/\sqrt{\rho}$ where the normalized far-field pattern is

$$E_y^{\rm ff}(\theta) = \cos\theta \sqrt{\frac{jk_0}{2\pi}}\, \tilde{E}_y(k_0 \sin\theta) \tag{4}$$

and θ is the angle measured from broadside.

The radiated power density (which is actually the power per unit angle for a one meter length along the y direction) is $P(\theta) = |E_y^{\rm ff}(\theta)|^2/(2\eta_0)$ so that at broadside we have

$$P(0) = \frac{k_0\eta_0}{4\pi}\frac{\sin^2(k_0 h_{\rm s}\sqrt{\varepsilon_{\rm r}})}{\left|\sqrt{\varepsilon_{\rm r}}\cos(k_0 h\sqrt{\varepsilon_{\rm r}}) + j\sin(k_0 h\sqrt{\varepsilon_{\rm r}})\right|^2}. \quad (5)$$

The first goal is to find the maximum of $P(0)$ as a function of h, keeping the frequency f fixed. Since $|\varepsilon_{\rm r}| < 1$, in order to maximize $P(0)$ we require that the sine term in the denominator of (5) vanishes, which is equivalent to requiring that the slab height h be a multiple of half a wavelength inside the slab ($\lambda_\varepsilon = \lambda_0/\sqrt{\varepsilon_{\rm r}}$), i.e.

$$k_0 h\sqrt{\varepsilon_{\rm r}(f)} = n\pi \qquad n = 1, 2, \ldots. \quad (6)$$

The location of the source should be chosen in order to maximize the numerator in (5), i.e., $h_{\rm s}$ should be an odd multiple of $\lambda_\varepsilon/4$. (For the thinnest slab, $n = 1$, this corresponds to placing the source in the middle of the slab.)

Second, we wish to find the maximum of $P(0)$ as a function of f, keeping the slab height h fixed. It can be observed that the variation of $P(0)$ is mainly due to its denominator, since the numerator is a slowly-varying function of f. Therefore, with the same reasoning as above, it can be concluded from (6) that the optimum frequency is $f_{\rm opt} = nc/(2h\sqrt{\varepsilon_{\rm r}(f_{\rm opt})})$ (where c is the speed of the light in vacuum). This is actually an implicit equation, since the relative permittivity $\varepsilon_{\rm r}$ is a function of frequency f. By using (1), an explicit expression for $f_{\rm opt}$ can be obtained in terms of the plasma frequency $f_{\rm p}$ and the slab height h as

$$f_{\rm opt} = \sqrt{f_{\rm p}^2 + \frac{n^2c^2}{4h^2}}. \quad (7)$$

The validity of condition (6) is approximately independent of the location of the source $h_{\rm s}$, although the level of radiated power density at broadside strongly depends on it, being maximum when h_s is an odd multiple of $\lambda_\varepsilon/4$.

When the optimum condition (6) is satisfied and $h_{\rm s}$ is an odd multiple of $\lambda_\varepsilon/4$, the power density at broadside is inversely proportional to the relative permittivity:

$$P(0) = P_{\max} = \frac{k_0\eta_0}{4\pi}\frac{1}{\varepsilon_{\rm r}(f_{\rm opt})}. \quad (8)$$

This result clearly shows the importance of metamaterials with *low* $\varepsilon_{\rm r}$ to obtain strong field values at broadside.

The validity of the optimum condition (6) can be verified by considering a specific structure with, e.g., a plasma frequency $f_{\rm p} = 20$ GHz. In Fig. 2(a), the power density radiated at broadside $P(0)$ by a unit-amplitude electric line source is reported as a function of the slab height h, when the operating frequency has been chosen to be $f = 20.155$ GHz, such that $\varepsilon_{\rm r} = 0.015$ and $\lambda_\varepsilon = 120$ mm, and the source is located at $h_{\rm s} = \lambda_\varepsilon/4 = 30$ mm. The power density is expressed in dB (relative to one W/m $\cdot$ rad). It can be seen that $P(0)$ is a strictly periodic function of h and shows maxima when h is an integer multiple of $\lambda_\varepsilon/2 = 60$ mm.

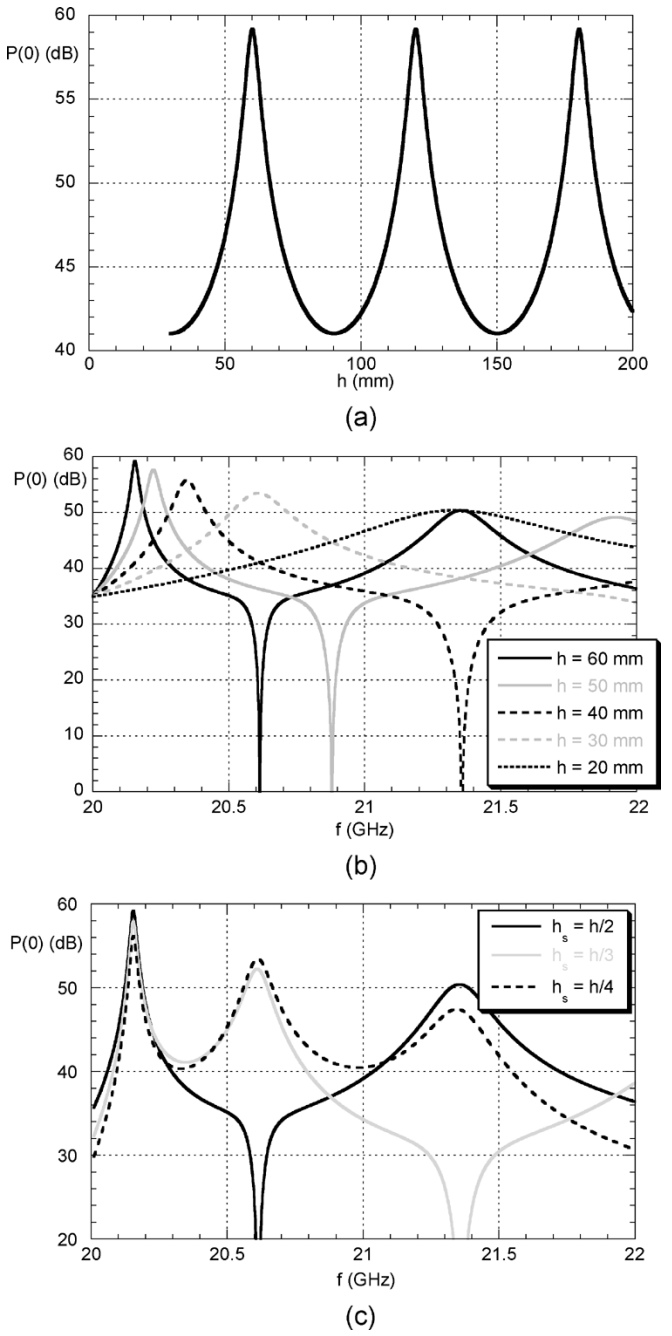

Fig. 2. Power density radiated at broadside $P(0)$ by a unit amplitude electric line source placed in a grounded metamaterial slab as in Fig. 1(b) with $f_{\rm p} = 20$ GHz. (a) As a function of the slab height h at the frequency $f = 20.155$ GHz and with $h_{\rm s} = 30$ mm. (b) As a function of the frequency f for different values of the slab height h with $h_{\rm s} = h/2$. (c) As a function of the frequency f for different values of the source location $h_{\rm s}$ with $h = 60$ mm.

In Fig. 2(b), the power density radiated at broadside $P(0)$ is reported as a function of the frequency f for different values of the slab height h, with the source located at $h_{\rm s} = h/2$. It can be observed that, as expected from (6), for each value of h, the maxima of $P(0)$ are located at frequencies for which h is an odd integer multiple of $\lambda_\varepsilon/2$ (note that, since the wavelength in the slab varies rapidly with frequency, the frequencies at which $h = \lambda_\varepsilon/2$ and $h = \lambda_\varepsilon$ are actually fairly close). Furthermore, it can be seen that, when h is equal to even multiples of λ_ε, zero

power is radiated at broadside; in fact, in the latter case, the numerator of (5) is zero since $h_s = h/2$ is an even multiple of $\lambda_\varepsilon/4$. In Fig. 2(b) it can also be observed that maxima corresponding to values of $n > 1$ in (6) are lower than the maximum corresponding to $n = 1$. This is consistent with (8) since higher values of n correspond to higher frequencies and thus to higher values of ε_r.

In Fig. 2(c), $P(0)$ is reported as a function of the frequency f for different values of the source location h_s, keeping the slab height fixed at $h = 60$ mm. As expected, the frequencies at which $P(0)$ is maximum do not appreciably depend on h_s, even though the maximum level of $P(0)$ decreases by decreasing the distance of the source from the ground plane, starting from $h_s = h/2$. At the peaks the power density for the case $h_s = h/4$ is lower than for the case $h_s = h/2$ by 3 dB, as expected (except for the second peak at 20.6 GHz, where the pattern for $h_s = h/2$ has a null instead of a peak, as explained previously).

It is also interesting to study the behavior of the directivity at broadside, defined as

$$D = \frac{2\pi \left|E_y^{\text{ff}}(0)\right|^2}{\int_{-\frac{\pi}{2}}^{\frac{\pi}{2}} \left|E_y^{\text{ff}}(\theta)\right|^2 \mathrm{d}\theta} \tag{9}$$

as a function of h and f. In Fig. 3(a), the directivity at broadside D is reported as a function of h, for a structure as in Fig. 2(a). In Fig. 3(b) and (c), D is reported as a function of the frequency f for the same cases considered in Fig. 2(b) and (c), respectively. Although the directivity D is not strictly periodic in h, it can be observed in Fig. 3(a) that it is also maximized when $h = n\lambda_\varepsilon/2$ with n odd. Moreover, condition (6) also maximizes the directivity as a function of frequency [see Fig. 3(b)], independently of the location of the source (see Fig. 3(c), where $h = 60$ mm).

The behavior of the total radiated power P_{tot} (expressed in dB relative to one W/m) as a function of h or f is shown in Fig. 4, for the same cases already considered in Figs. 2 and 3. It can be observed that P_{tot} attains local maxima for the same values of the slab height and frequency as the radiated power density at broadside and directivity.

As a final remark, by a comparison of Figs. 2(b) and 3(b), one may note that a bandwidth definition based on the directivity D would be larger than that defined using the radiated power density $P(0)$. The bandwidth is analyzed analytically in the next Section.

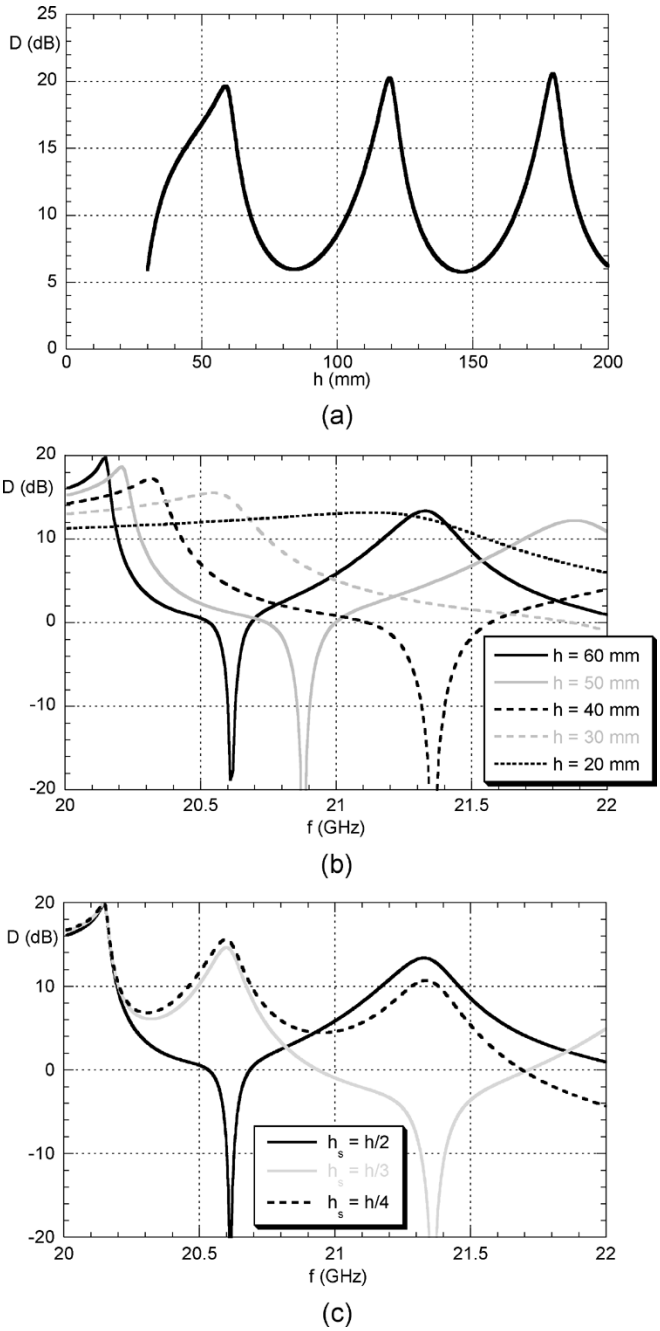

Fig. 3. Directivity at broadside D for the structure in Fig. 1(b). (a) As a function of the slab height h for the structure in Fig. 2(a). (b) As a function of the frequency f for different values of h with $h_s = h/2$, as in Fig. 2(b). (c) As a function of the frequency f for different values of h_s with $h = 60$ mm, as in Fig. 2(c).

B. Bandwidth for Radiation at Broadside

We consider now the bandwidth for radiation at broadside, defined as the frequency range $f_{3\,\text{dB}}^- < f < f_{3\,\text{dB}}^+$ where the power density level $P(0)$ radiated at broadside is within 3 dB of its maximum $P_{\max}$ in (8), reached at $f = f_{\text{opt}}$. As shown in Section II-A, the maximum power density at broadside is achieved when (7) is satisfied. To calculate the power fractional bandwidth (FBW) at broadside, we search the frequencies $f_{3\,\text{dB}}^{\pm} = f_{\text{opt}} + \delta f_{\pm}$ such that the broadside radiated power density $P(0)$ in (5) is one half of its maximum value $P_{\max}$ in (8). By using a Taylor expansion in a neighborhood of $f = f_{\text{opt}}$ of the trigonometric functions and $\varepsilon_r(f)$ in (5) truncated to the second-order terms in δf, and by assuming $|\varepsilon_r(f_{\text{opt}})| \ll 1$, after some algebra a second-order equation for δf is obtained, assuming the case $n = 1$

$$\delta f^2 + \frac{2f_{\text{opt}}^3 \varepsilon_r^2(f_{\text{opt}})}{\pi^2 f_p^2}\delta f - \frac{f_{\text{opt}}^6 \varepsilon_r^3(f_{\text{opt}})}{\pi^2 f_p^4} = 0. \tag{10}$$

The middle term in the above equation is neglected since it is the smallest (justified from the final solution for δf). From the two solutions of (10), the FBW is thus

$$\text{FBW} = \frac{f_{3\,\text{dB}}^+ - f_{3\,\text{dB}}^-}{f_{\text{opt}}} \simeq \frac{1}{f_{\text{opt}}} \frac{2f_{\text{opt}}^3 \varepsilon_r^{\frac{3}{2}}(f_{\text{opt}})}{\pi f_p^2} \simeq \frac{2\varepsilon_r^{\frac{3}{2}}(f_{\text{opt}})}{\pi} \tag{11}$$

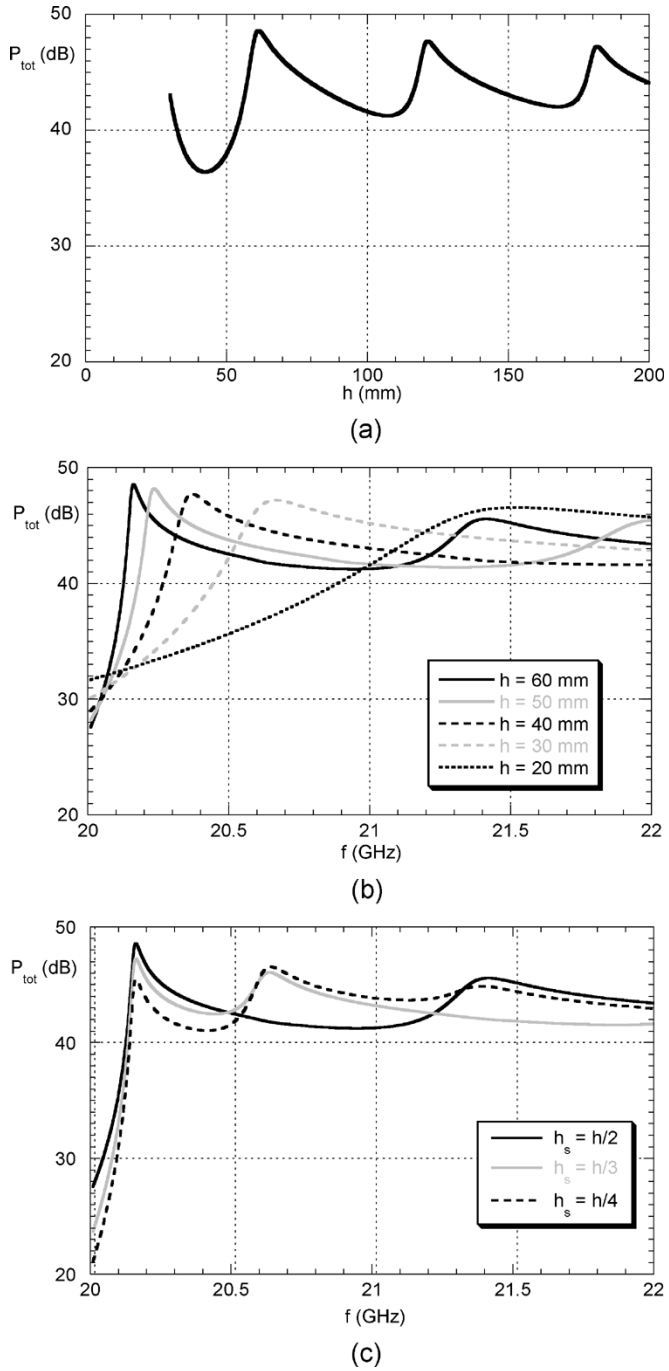

Fig. 4. Total radiated power for the structure in Fig. 1(b). (a) As a function of the slab height h for the structure in Fig. 2(a). (b) As a function of the frequency f for different values of h with $h_{\rm s} = h/2$, as in Fig. 2(b). (c) As a function of the frequency f for different values of $h_{\rm s}$ with $h = 60$ mm, as in Fig. 2(c).

where the last approximation is valid for slab heights such that $h \gg c/(2f_{\rm p})$ so that $f_{\rm opt} \simeq f_{\rm p}$. Alternatively, by means of (1) and (7), the FBW can be expressed in terms of the plasma frequency $f_{\rm p}$ and the slab height h, i.e.,

$$\mathrm{FBW} = \frac{c^3}{4\pi f_{\rm p}^3}\frac{1}{h^3}. \tag{12}$$

Fig. 5 shows a comparison between the approximate result (12) (*gray solid line*) and the exact power fractional bandwidth

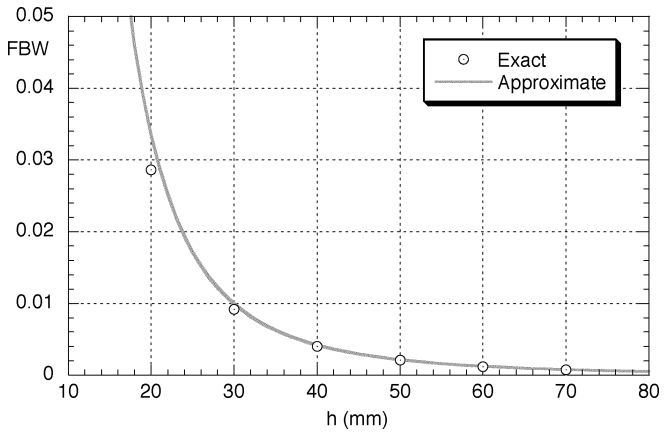

Fig. 5. Comparison between the exact power fractional bandwidth at roadside (evaluated by means of the frequencies $f_{3\,\rm dB}^{\pm}$ and $f_{\rm opt}$ calculated numerically, *black circles*) and the approximate formula (calculated by means of (12), *gray dashed line*) as a function of the slab height h for the structure in Fig. 2(a).

FBW at broadside evaluated by means of the frequencies $f_{3\,\rm dB}^{\pm}$ and $f_{\rm opt}$ calculated numerically (*black circles*) as functions of the slab height h for a structure as in Fig. 2(a). As can be observed, very good agreement is obtained starting from about $h = 20$ mm.

C. Far-Field Pattern and Radiation Off Broadside

When the operating frequency differs from $f_{\rm opt}$, the far-field pattern changes in two possible ways: either a beam with a single peak at broadside is radiated (however with a smaller amplitude with respect to the optimum case) or a beam with two (or more) peaks off broadside is produced.

This behavior is illustrated in Fig. 6(a) where the radiation pattern of a structure as in Fig. 2 with $h = 60$ mm (such that $f_{\rm opt} = 20.155$ GHz) and $h_{\rm s} = h/2$ is shown at different frequencies. When $f = 20.1$ GHz (i.e., below $f_{\rm opt}$) the beam points at broadside, whereas at $f = 21$ GHz (i.e., above $f_{\rm opt}$) two narrow maxima are obtained at $\theta \simeq \pm 16.3°$. When the frequency is further increased [e.g., at $f = 23$ GHz in Fig. 6(a)] additional beams are produced.

By keeping the frequency and source location fixed at $f = 20.155$ GHz and $h_{\rm s} = \lambda_\varepsilon/4 = 30$ mm, respectively, and by varying the slab height, the radiation pattern changes, as illustrated in Fig. 6(b). It can also be noted that in this case, when the optimum condition $h = \lambda_\varepsilon/2$ [see (6)] is satisfied, the far-field pattern has a peak at broadside with the maximum amplitude. When $h < \lambda_\varepsilon/2$, the beam still points at broadside; furthermore, when $h = h_{\rm s} = \lambda_\varepsilon/4$, a very broad beam is radiated, almost constant in the angular range shown. When $h > \lambda_\varepsilon/2$, a beam with two peaks off broadside is produced, though other peaks may also appear off broadside (e.g., for $h = \lambda_\varepsilon$). From numerical experiments, we find that increasing the slab height increases the pointing angle, though it remains limited by the critical angle $\theta_{\rm c} = \sin^{-1}\sqrt{\varepsilon_{\rm r}} \simeq 7.12°$. This is explained in Section III-C.

All the radiative properties shown here are explained in the next section by means of modal properties of leaky waves supported by the grounded metamaterial slab.

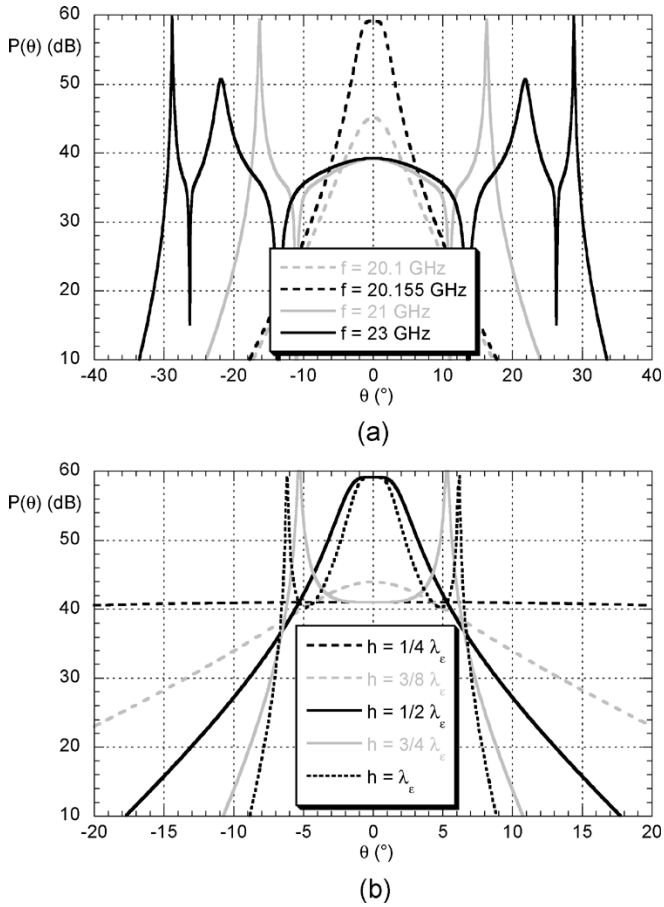

Fig. 6. Radiation pattern $P(\theta)$ for the structure as in Fig. 1(b). (a) For different frequencies with $h = 60$ mm and $h_s = h/2$. (b) For different slab heights with $f = 20.155$ GHz and $h_s = \lambda_\varepsilon/4 = 30$ mm.

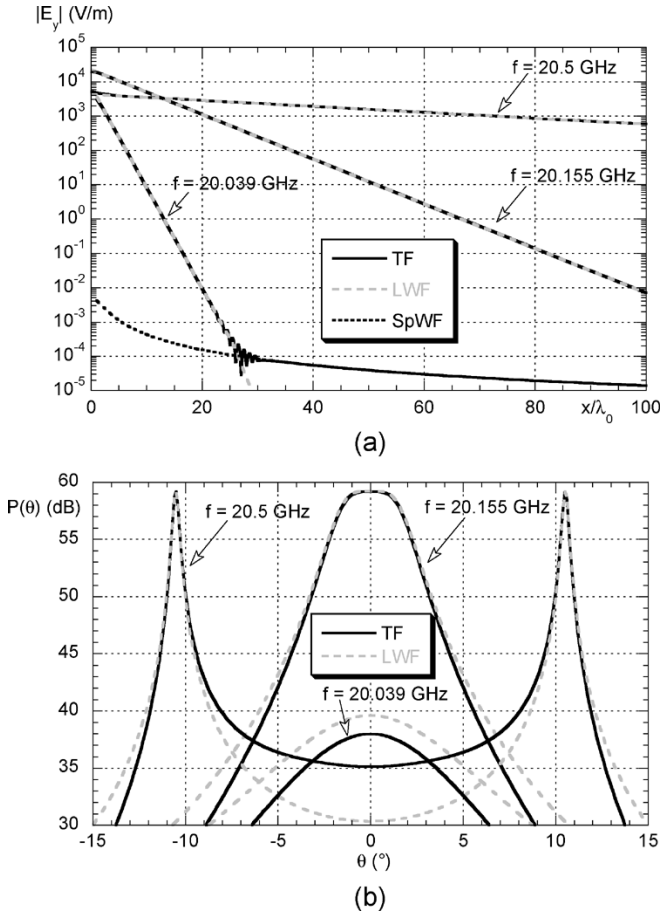

Fig. 7. Comparison between the total field (TF) and the leaky-wave field (LWF) for the structure in Fig. 6(a) at $f = 20.039$, $f = 20.155$, and $f = 20.5$ GHz. (a) Amplitude of the electric field at the air-slab interface as a function of the normalized distance from the source x/λ_0. (b) Radiation pattern $P(\theta)$.

III. Leaky-Wave Explanation of the Directive Radiation

The high-directivity properties at broadside of a grounded plasma slab have been explained by Enoch *et al.* with a simple ray-optic picture of the radiation phenomena based on mode matching at the boundary of the slab, supported with rigorous numerical calculations [33]. We briefly recall their explanation: if the refractive index of the slab is positive and much lower than one (near zero), the rays emitted by the source are refracted at the air-slab interface with transmitted angles belonging to a small angular range between broadside and the critical angle θ_c. Therefore, an enhancement of the directivity at broadside with respect to ordinary dielectric slabs can be expected; moreover, by varying frequency, the maximum of the radiation pattern is constrained to lie inside the above-mentioned angular range. This explanation provides important physical insight into the operation of the antenna, although a further understanding can be obtained by examining the guided waves supported by the structure. It is demonstrated here that the narrow-beam effect is due to the excitation of a leaky wave. In particular, the interesting refractive property outlined in [33] is valid for the direct field excited by the source, and thus also for the various blurred "images" reflected by the ground plane and the top-material interface. However, what makes the structure extremely directive is not only the refractive effect, but also the fact that all the waves (direct and reflected) produced by the source add constructively to produce a strong radiation at broadside. From a guided-wave point of view, these wave fields are all part of a leaky-wave field that is excited by the source and propagates away from the source in the $\pm x$ directions. This is explained and quantified in the following.

Remarkably, for a similar problem (but a completely different application), Tamir and Oliner showed in 1962 [35] that the radiation pattern of an excited plasma slab was due to the excitation of a leaky wave with a small attenuation constant and a phase constant lower than $\sin\theta_c$. Moreover, they showed that, by increasing the frequency, additional beams can originate from broadside due to the excitation of higher-order leaky waves, as we noticed in Fig. 6(a). Note that since ε_r increases with frequency, the angular range defined by the critical angle broadens when the frequency is increased. On the contrary, by keeping the frequency fixed as in Fig. 6(b), the critical angle does not change. Moreover, when $h = h_s = \lambda_\varepsilon/4$ a very broad nondirective beam is radiated since in this case the involved leaky wave is poorly excited and the field is mainly due to the space wave [43].

In order to demonstrate the dominant role of the leaky-wave field in determining these radiation characteristics, a comparison between the exact total field (TF) and the leaky-wave field (LWF) is presented in Fig. 7 for a structure with $f_p = 20$ GHz, $h = 60$ mm, and $h_s = h/2$, such that the optimum frequency

for maximum power density at broadside is, from (7), $f_{\rm opt} = 20.155$ GHz. In particular, in Fig. 7(a), a comparison between the TF and the LWF excited at the slab-air interface is shown for three different frequencies above $f_{\rm p}$ as a function of the normalized distance from the source x/λ_0. The TF is calculated by numerically evaluating the integral in (2); the LWF is evaluated as the residue contribution to the integral in (2) at the dominant complex leaky-wave pole at $k_x = k_{\rm LW} \equiv \beta - j\alpha$ of the spectral field (3) (i.e., the one with the lowest attenuation constant α) [43], and it has the simple expression

$$E_y^{\rm LW}(x) = E_0\, e^{-jk_{\rm LW}|x|} \tag{13}$$

with $E_0 = -j{\rm Res}[\tilde{E}_y(k_x)]_{k_x=k_{\rm LW}}$. In general, when α has sufficiently low values, the LWF is dominant on the air-slab interface, provided that the residue is not too small [43]. In Fig. 7(a), it can be seen that the LWF is completely coincident with the TF in the entire spatial range both at $f = 20.155$ GHz (where the beam peak is off broadside) and $f = 20.5$ GHz (corresponding to maximum radiation off broadside), thus revealing its dominant character. On the other hand, at $f = 20.039$ GHz, (i.e., below the optimum frequency) the LWF is dominant only up to $x \simeq 25\lambda_0$; for larger distances from the source, a change from the exponential behavior of the LWF to the algebraic decay of the space-wave field (SpWF) is observed [42]. Above the interface the domain of existence of the leaky-wave field is restricted to an angular region $|\theta| > \theta_{\rm LW}$, where $\theta_{\rm LW}$ is determined from the propagation constant of the leaky wave, as in standard slab problems [43]. The SpWF along the interface is calculated by performing the integration in (2) along a vertical path that goes around the branch point at k_0, which becomes a steepest-descent path in the limit of large x/h [42], i.e., when the integrand $\tilde{E}_y(k_x)$ is slowly varying with respect to $\exp(-jk_x x)$. The SpWF in Fig. 7(a) is reported only for $f = 20.039$ GHz since it remains almost the same at the other two frequencies. It should be noted that the SpWF always constitutes the dominant asymptotic contribution to the TF for large distances from the source, although this is visible only for $f = 20.039$ GHz in the distance range shown in Fig. 7(a).

In Fig. 7(b), the relevant radiation patterns are compared; also in this case the agreement between the TF and the LWF is excellent both at $f = 20.155$ GHz and $f = 20.5$ GHz, whereas, at $f = 20.039$ GHz, a discrepancy due to the nonnegligible contribution of the SpWF is observed.

Knowledge of the fact that the aperture field is dominated by a leaky-wave that is attenuating away the source is important to determine where these structures can be truncated without affecting the radiative features.

A. Leaky-Wave Explanation of the Optimum Radiation Condition

In this section our goal is to show that the optimum condition (6) or (7) implies the presence of a TE leaky wave with small and nearly equal values of the phase and the attenuation constants. Let us consider then the dispersion equation for TE modes, which can be obtained by equating the denominator of (3) to zero. This equation can be written in terms of the normalized leaky-wave propagation constant $\hat{k}_{\rm LW} = \hat{\beta} - j\hat{\alpha}$ as

$$\frac{1}{\sqrt{1-\hat{k}_{\rm LW}^2}} + j\frac{1}{\sqrt{\varepsilon_{\rm r}-\hat{k}_{\rm LW}^2}}\tan\left(k_0 h\sqrt{\varepsilon_{\rm r}-\hat{k}_{\rm LW}^2}\right) = 0 \tag{14}$$

where a caret ($\hat{}$ symbol) indicates normalization with respect to k_0. By assuming $|\hat{k}_{\rm LW}^2| \ll \varepsilon_{\rm r} < 1$ and by using a Taylor expansion of the square-root functions in (14), we have

$$\sqrt{\varepsilon_{\rm r}}\left(1-\frac{\hat{k}_{\rm LW}^2}{2\varepsilon_{\rm r}}\right) + j\left(1-\frac{\hat{k}_{\rm LW}^2}{2}\right)\times \tan\left(k_0 h\sqrt{\varepsilon_{\rm r}} - k_0 h\frac{\hat{k}_{\rm LW}^2}{2\sqrt{\varepsilon_{\rm r}}}\right) \simeq 0. \tag{15}$$

By taking into account the optimum condition (6), by approximating the tangent using $\tan(n\pi - x) \simeq -x$, and neglecting higher-order powers in $\hat{k}_{\rm LW}$, (15) can be approximated as

$$\sqrt{\varepsilon_{\rm r}}\left(1-\frac{\hat{k}_{\rm LW}^2}{2\varepsilon_{\rm r}}\right) - j\frac{n\pi\hat{k}_{\rm LW}^2}{2\varepsilon_{\rm r}} \simeq 0 \tag{16}$$

and from (16) we obtain an approximate asymptotic expression for $\hat{k}_{\rm LW}^2$:

$$\hat{k}_{\rm LW}^2 \simeq \frac{2\varepsilon_{\rm r}^{\frac{3}{2}}(\sqrt{\varepsilon_{\rm r}} - jn\pi)}{\varepsilon_{\rm r} + n^2\pi^2}. \tag{17}$$

Taking the real and imaginary parts

$$\begin{aligned}\hat{\beta}^2 - \hat{\alpha}^2 &= \frac{2\varepsilon_{\rm r}^2}{\varepsilon_{\rm r}+n^2\pi^2}\\ \hat{\beta}\hat{\alpha} &= \frac{n\pi\varepsilon_{\rm r}^{\frac{3}{2}}}{\varepsilon_{\rm r}+n^2\pi^2}.\end{aligned} \tag{18}$$

In the limit of small $\varepsilon_{\rm r}$, the right-hand side of the first of (18) can be neglected with respect to the right-hand side of the second of (18); thus it is concluded that the optimum condition (6) implies

$$\hat{\beta} \simeq \hat{\alpha} \simeq \sqrt{\frac{\varepsilon_{\rm r}^{\frac{3}{2}}}{n\pi}}. \tag{19}$$

For the analysis to be consistent we require that the absolute value of $\hat{k}_x$ thus obtained satisfies the initial assumption $|\hat{k}_x| \ll \sqrt{\varepsilon_{\rm r}}$, and, from (19) with $n = 1$, this is equivalent to

$$\varepsilon_{\rm r} \ll \frac{\pi^2}{4} \simeq 2.467 \tag{20}$$

which defines the range of "small" $\varepsilon_{\rm r}$. The relative permittivity $\varepsilon_{\rm r}$ in (19) has then to be evaluated at the optimum frequency $f_{\rm opt}$ in (7), i.e.

$$\varepsilon_{\rm r}(f_{\rm opt}) = 1 - \frac{f_{\rm p}^2}{f_{\rm opt}^2} = 1 - \frac{f_{\rm p}^2}{f_{\rm p}^2 + \frac{n^2c^2}{4h^2}} \simeq \frac{n^2c^2}{4f_{\rm p}^2h^2} \tag{21}$$

where the last approximation is valid for slab heights such that $h \gg nc/(2f_{\rm p})$. By substituting (21) into (19) we finally obtain

$$\hat{\beta} \simeq \hat{\alpha} \simeq \sqrt{\frac{n^2c^3}{8\pi f_{\rm p}^3h^3}}. \tag{22}$$

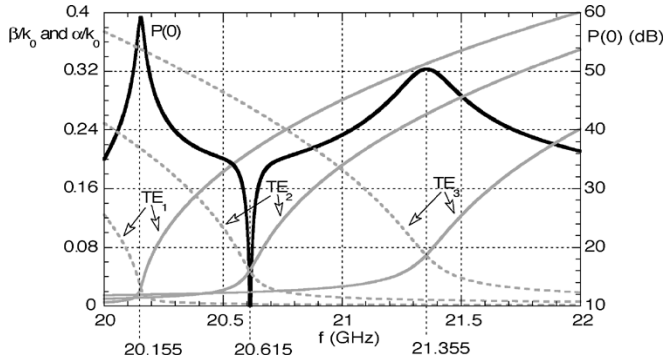

Fig. 8. Normalized leaky-wave phase (β/k_0, *solid gray lines*) and attenuation (α/k_0, *dashed gray lines*) constants and power density radiated at broadside ($P(0)$, *solid black line*) as a function of frequency f for a structure in Fig. 6(a). The exact frequencies for which $P(0)$ is maximum or minimum are indicated at the bottom of the figure.

In order to validate the previous analysis, in Fig. 8 the dispersion curves of the first three leaky modes (labeled as TE_1, TE_2, TE_3) are reported together with the power density radiated at broadside $P(0)$ as a function of frequency for a structure as in Fig. 6(a) (i.e., $h = 60$ mm, $h_\mathrm{s} = h/2$, $f_\mathrm{p} = 20$ GHz, $f_\mathrm{opt} = 20.155$ GHz). It can be seen that $P(0)$ has its maxima in correspondence with the frequencies (explicitly labeled in Fig. 8) for which a leaky mode has equal values of its phase and attenuation constants. (However, the power density is minimum rather than maximum at the crossing point for the phase and attenuation constants of the TE_2 leaky mode because the source is in the middle of the substrate, and does not excite the TE_2 leaky mode at this frequency.) Moreover, the approximate values for both the optimum frequencies [obtained with (7)] and the leaky-mode phase and attenuation constants [obtained with (22)] are in excellent agreement with the exact ones calculated numerically.

Finally, expressions for P_max and FBW can be obtained in terms of the normalized attenuation constant $\hat{\alpha}$ at the optimum frequency f_opt. In fact, from (8) and (12), by means of (22), we have

$$P_\mathrm{max} \simeq \frac{k_0\eta_0}{4\pi^{\frac{5}{3}}}\frac{1}{\hat{\alpha}^{\frac{4}{3}}} \tag{23}$$

and

$$\mathrm{FBW} \simeq 2\hat{\alpha}^2 \tag{24}$$

where $\hat{\alpha}$, given in (22), can be controlled by varying the slab height h and the plasma frequency f_p, which in turn depends on the small scale geometry of the chosen metamaterial medium.

If we define the enhancement of power density at broadside E_P of the antenna as the ratio between its maximum power density radiated at broadside and the power density radiated at broadside by a unit amplitude electric line source in free space [which is equal to $k_0\eta_0/(16\pi)$], we have

$$E_\mathrm{P} \simeq \frac{4}{(\sqrt{\pi}\hat{\alpha})^{\frac{4}{3}}}. \tag{25}$$

Therefore, the enhancement-fractional-bandwidth product EFBW at broadside is

$$\mathrm{EFBW} = E_\mathrm{P}\cdot\mathrm{FBW} \simeq \frac{8}{\pi^{\frac{2}{3}}}\hat{\alpha}^{\frac{2}{3}}. \tag{26}$$

This means that, by letting the normalized attenuation constant $\hat{\alpha}$ have small values (e.g., through the use of thick slabs), a large radiated power density at broadside (25) can be obtained, but at the expense of having a very small fractional bandwidth (24). Note that the enhancement factor E_P increases as $\hat{\alpha}$ decreases, though the bandwidth FBW decreases even faster.

B. Maximum Directivity at Broadside

On the basis of the leaky-wave analysis of the grounded metamaterial slab, an extremely simple formula can be obtained for the directivity at broadside defined as in (9). In fact, by assuming that the field at the air-slab interface is dominated by the leaky-wave field (13), for the spectral electric field we have [43]

$$\tilde{E}_y(\hat{k}_x) = \frac{2jE_0k_0\hat{k}_\mathrm{LW}}{\hat{k}_x^2 - \hat{k}_\mathrm{LW}^2}. \tag{27}$$

At the optimum frequency we have $\hat{\beta} = \hat{\alpha}$, so that $\hat{k}_\mathrm{LW} = \hat{\alpha}(1-j)$ and

$$\left|\tilde{E}_y(\hat{k}_x)\right|^2 = \frac{8|E_0|^2k_0^2\hat{\alpha}^2}{\hat{k}_x^4 + 4\hat{\alpha}^4}. \tag{28}$$

Therefore, from (9), by letting $\hat{k}_x = \sin\theta$, the directivity at broadside at the optimum frequency can be written as

$$D = \frac{2\pi}{4\alpha^4}\frac{1}{\int_{-1}^{1}\frac{\sqrt{1-\hat{k}_x^2}}{\hat{k}_x^4+4\hat{\alpha}^4}\mathrm{d}\hat{k}_x}. \tag{29}$$

The integral in the denominator of (29) can be evaluated in a closed form (see, e.g., [44])

$$\int_{-1}^{1}\frac{\sqrt{1-\hat{k}_x^2}}{\hat{k}_x^4+4\hat{\alpha}^4}\mathrm{d}\hat{k}_x = \frac{\pi}{4\hat{\alpha}^3}\sqrt{-2\hat{\alpha}^2+\sqrt{4\hat{\alpha}^4+1}} \tag{30}$$

so that, from (29) and (30), we finally obtain

$$D = \frac{2}{\hat{\alpha}\sqrt{-2\hat{\alpha}^2+\sqrt{4\hat{\alpha}^4+1}}} \simeq \frac{2}{\hat{\alpha}} \simeq \sqrt{\frac{32\pi f_\mathrm{p}^3h^3}{c^3}} \tag{31}$$

where the last approximations hold in the limit of small $\hat{\alpha}$.

As a validation of the latter result, a comparison between the exact directivity at broadside [calculated by means of (9)] and the approximate one [calculated by means of (31)] as a function of the slab height h is reported in Fig. 9 for a grounded metamaterial slab with $f_\mathrm{p} = 20$ GHz; for each value of h, the operating frequency is f_opt and the source is located at $h_\mathrm{s} = h/2$. It can be seen that the agreement between the two curves is excellent.

From (31) and (24) it is seen that the directivity-fractional-bandwidth product DFBW is $\mathrm{DFBW} = D\cdot\mathrm{FBW} \simeq 2\hat{\alpha}$, which becomes small as the directivity increases (α decreases), even faster than does the product EFBW [from (26)].

C. Angular Limits of the Directive Radiation

As mentioned at the beginning of this section, the direction of maximum radiation is constrained to lie inside the angular region between broadside and the critical angle θ_c. Here we aim to show that this feature is related to properties of the leaky-wave poles in the limit of large slab height h. In particular, as h increases, the normalized phase constant $\hat{\beta}$ of each leaky mode increases, approaching a limiting value of $\hat{\beta} = \sqrt{\varepsilon_\mathrm{r}}$. The precise

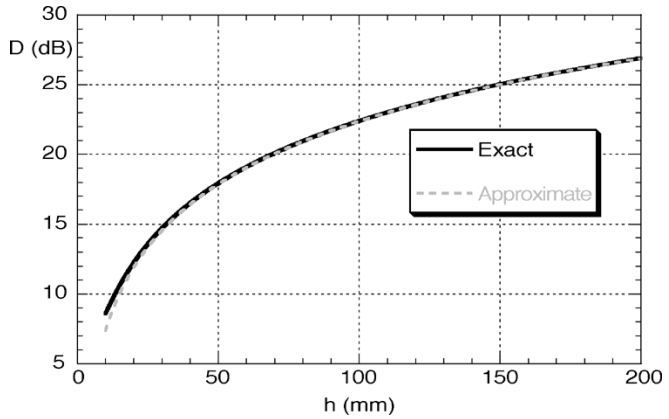

Fig. 9. Comparison between the exact directivity at broadside (calculated by means of (9), *black solid line*) and its approximation (calculated by means of (31), *gray dashed line*) as a function of the slab height h for a structure as in Fig. 2. For each value of h, the operating frequency is $f_{\rm opt}$ (with $n = 1$) and the source is located at $h_{\rm s} = h/2$.

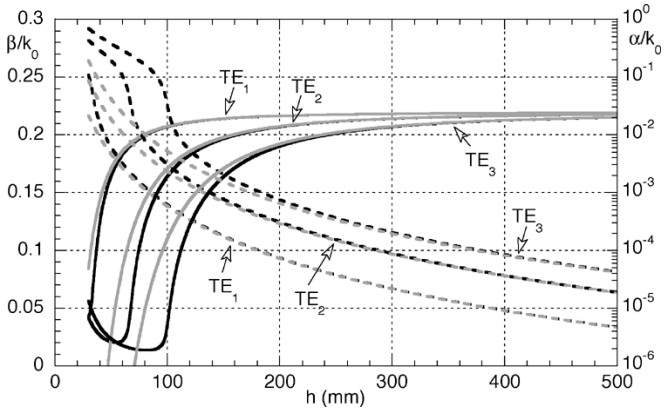

Fig. 10. Normalized phase and attenuation constants of the $\rm TE_1$, $\rm TE_2$, and $\rm TE_3$ leaky modes as functions of the slab height h for a structure in Fig. 2 at the operating frequency $f = 20.5$ GHz. Legend for phase constants β/k_0: *black solid line*, exact; *gray solid line*, approximate (Eq. (34)). Legend for attenuation constants α/k_0: *black dashed line*, exact; *gray dashed line*, approximate [Eq. (34)].

manner in which this happens is demonstrated by the following asymptotic analysis (see also [38]).

By letting $\hat{k}_x = \sqrt{\varepsilon_{\rm r}} - j\delta$, from (14) it can be seen that, for the second addend to have a limit for $h \to \infty$, δ must be infinitesimal and the argument of the tangent must tend to $n\pi$, $n > 0$. Equation (14) can thus be approximated as

$$\frac{1}{\sqrt{1-\varepsilon_{\rm r}}} + j\frac{1}{\sqrt{2j\sqrt{\varepsilon_{\rm r}}\delta}}(k_0 h\sqrt{2j\sqrt{\varepsilon_{\rm r}}\delta} - n\pi) \simeq 0 \qquad (32)$$

from which δ can be obtained as

$$\delta \simeq -\frac{n^2\pi^2}{2j\sqrt{\varepsilon_{\rm r}}\left(\frac{1}{1-\varepsilon_{\rm r}} - k_0^2 h^2\right) - 4\frac{k_0 h\sqrt{\varepsilon_{\rm r}}}{\sqrt{1-\varepsilon_{\rm r}}}}. \qquad (33)$$

By separating into real and imaginary parts, an approximate formula for the normalized phase and attenuation constants of the leaky wave can be obtained in the asymptotic limit of large h as

$$\hat{\beta} \simeq \sqrt{\varepsilon_{\rm r}} - \frac{n^2\pi^2}{2\sqrt{\varepsilon_{\rm r}}k_0^2}\frac{1}{h^2}$$
$$\hat{\alpha} \simeq \frac{n^2\pi^2}{\sqrt{\varepsilon_{\rm r}(1-\varepsilon_{\rm r})}k_0^3}\frac{1}{h^3}. \qquad (34)$$

It is thus analytically proved that, by increasing the slab height h and keeping the frequency fixed, the normalized phase constant $\hat{\beta}$ tends to $\sqrt{\varepsilon_{\rm r}}$ from lower values, while the normalized attenuation constant $\hat{\alpha}$ tends even more rapidly to zero. In terms of beams, this means that for a fixed frequency, increasing h causes the beam corresponding to a particular n-th leaky mode to scan from broadside to the critical angle $\theta_{\rm c}$, while its beamwidth (related to the attenuation constant) tends to zero.

In Fig. 10, the normalized phase (*solid lines*) and attenuation (*dashed lines*) constants of the $\rm TE_1$, $\rm TE_2$, and $\rm TE_3$ leaky modes as functions of the slab height h for a structure with $f_{\rm p} = 20$ GHz at the operating frequency $f = 20.5$ GHz are reported. In particular, it can be seen that all the normalized phase constants tend to $\sqrt{\varepsilon_{\rm r}} = 0.219$ and all the normalized attenuation constants tend to zero; moreover, the exact curves (*black lines*) and the approximate ones (*gray lines*, obtained from (34)) are in excellent agreement for sufficiently high values of h. This is in accordance with the explanation of the directive radiation based on the refractive properties provided in [33], and with our comments at the beginning of Section III.

D. Comparison With a Plasma Half Space

Further physical insight into the radiative properties of the grounded plasma slab can be gained through a comparison with a different configuration, i.e., a unit-amplitude electric line source placed in a plasma *half space* at a distance $h_{\rm s}$ from the air-plasma interface. In fact, when the plasma is transparent (i.e., when its relative permittivity is positive), the latter structure does not support surface or leaky modes, so that any enhancement of power density or directivity at broadside with respect to free space must be related to a purely geometrical optics effect.

This is explained by looking at the spectral electric field at the plasma-air interface

$$\tilde{E}_y(k_x) = -\frac{Z_0 Z_1}{Z_0 + Z_1} e^{-jk_{z1}h_{\rm s}} \qquad (35)$$

which does not have any pole but has instead *two pairs of branch points* on the real axis located at $\pm k_0$ and $\pm k_0\sqrt{\varepsilon_{\rm r}}$. The total field at the air-plasma interface, along with the x coordinate (Fig. 1), can thus be represented as the sum of two integral contributions from the steepest-descent paths surrounding these branch points, that have the form of vertical paths under the asymptotic assumption $x/h_{\rm s} \gg 1$. The contribution from the branch points at $\pm k_0\sqrt{\varepsilon_{\rm r}}$ is the *space wave*, i.e., the geometrical optics contribution, whereas the contribution from the branch points at $\pm k_0$ is the *lateral wave* [42, Sec. 5.5].

The lateral wave propagates along the interface $z = 0$ with a phase constant equal to k_0, but its amplitude strongly depends on the location of the source since this wave decays exponentially in the vertical z direction in the plasma region. It can thus be expected that its contribution to the total field at the plasma-air interface is negligible, unless the source is located very close to the interface.

On the other hand, the space wave propagates along the interface $z = 0$ with a phase constant equal to $k_0\sqrt{\varepsilon_{\rm r}}$, and thus it radiates into the upper half space producing a beam with a maximum at the critical angle $\theta_{\rm c} = \sin^{-1}\sqrt{\varepsilon_{\rm r}}$, regardless of the location of the source.

In Fig. 11(a) and (b), a comparison between the exact total field (TF), the lateral-wave field (LatWF), and the space-wave

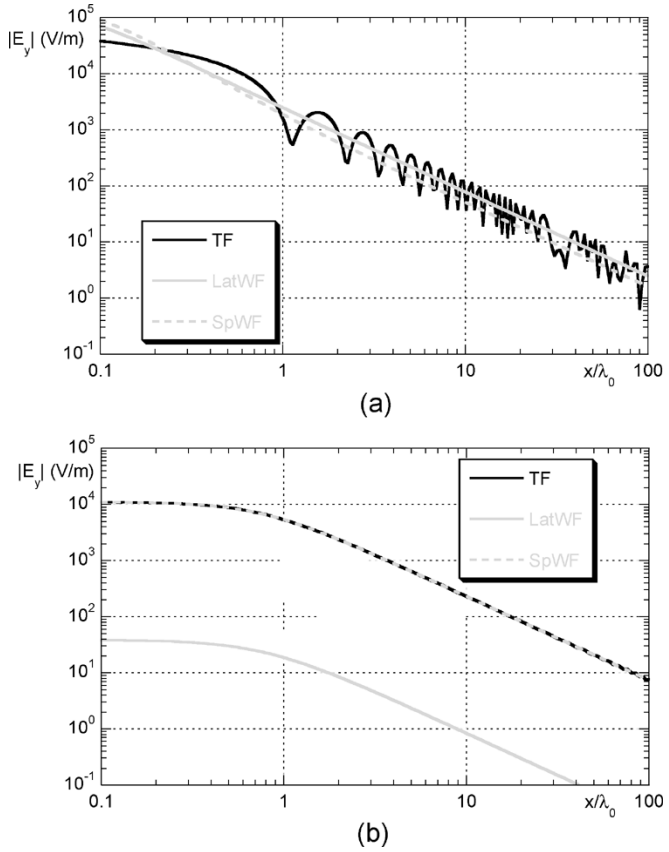

Fig. 11. Comparison among the exact total field (TF), the lateral-wave field (LatWF), and the space-wave field (SpWF) excited by an electric line source placed in a plasma half space at a distance $h_{\rm s}$ from the air-plasma interface, plotted along the interface as a function of the normalized distance x/λ_0 for (a) $h_{\rm s} = 0.01\lambda_\varepsilon$ and (b) $h_{\rm s} = 0.1\lambda_\varepsilon$. *Parameters*: $f_{\rm p} = 20$ GHz, $f = 20.015$ GHz.

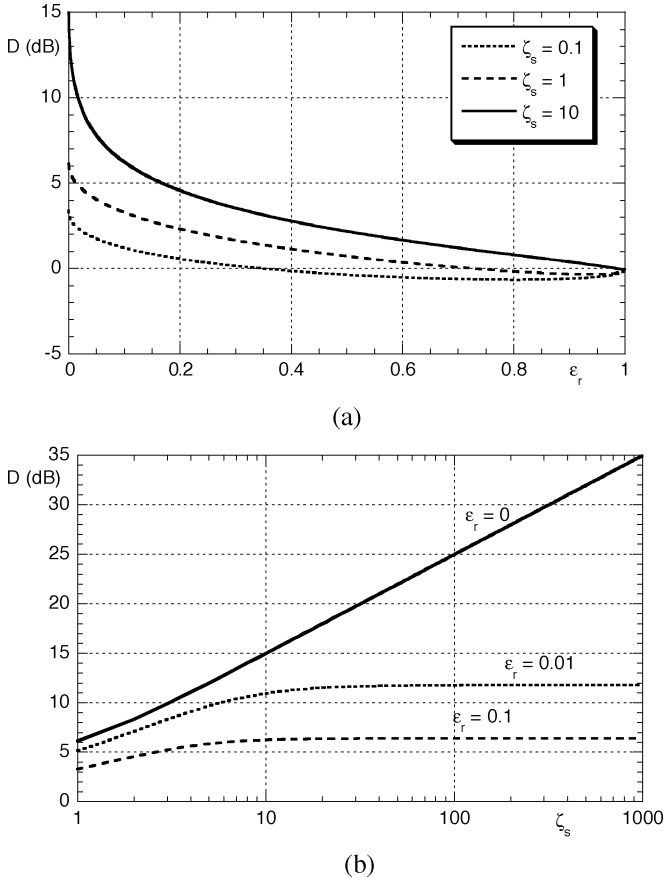

Fig. 12. Directivity at broadside D of a unit amplitude electric line source embedded in a plasma half space at a distance $h_{\rm s}$ from the air-plasma interface. (a) As a function of $\varepsilon_{\rm r}$ for different values of the normalized distance $\zeta_{\rm s} = k_0 h_{\rm s}$. (b) As a function of $\zeta_{\rm s}$ for different values of $\varepsilon_{\rm r}$.

field (SpWF) is presented for a half-space problem in which $f_{\rm p} = 20$ GHz and $f = 20.015$ GHz, where the source is located at $h_{\rm s} = 0.01\lambda_\varepsilon$ and $h_{\rm s} = 0.1\lambda_\varepsilon$, respectively. For these two cases, the asymptotic condition $x/h_{\rm s} \gg 1$ is met for $x \gg 0.25\lambda_0$ and $x \gg 2.5\lambda_0$, respectively; the steepest-descent paths for the LatWF and the SpWF then coincide with the vertical paths through the branch points k_0 and $k_0\sqrt{\varepsilon_{\rm r}}$, respectively, which are used in the numerical calculations. It can be noticed that, when the source is very close to the interface, as in Fig. 11(a), the LatWF and the SpWF are of the same order of magnitude and neither one correctly represents the TF (although their sum does, of course). On the other hand, by increasing the distance of the source from the interface, already at $h_{\rm s} = 0.1\lambda_\varepsilon$ the LatWF is negligible, and the TF is almost perfectly represented by the SpWF alone [see Fig. 11(b)].

From (35) the power density radiated in air can be obtained as

$$P(\theta) = \frac{k_0\eta_0}{4\pi}\cos^2\theta \frac{e^{-2k_0 h_{\rm s}\Im{\rm m}\{\sqrt{\varepsilon_{\rm r}-\sin^2\theta}\}}}{|\cos\theta + \sqrt{\varepsilon_{\rm r}-\sin^2\theta}|^2}. \tag{36}$$

From (36) it can be verified that the direction of maximum radiation is $\theta_{\rm c} = \sin^{-1}\sqrt{\varepsilon_{\rm r}}$, regardless of the location $h_{\rm s}$ of the source, so that the radiation pattern has a maximum at broadside only when $\varepsilon_{\rm r} = 0$. With reference to the power density radiated at broadside, the result is

$$P(0) = \frac{k_0\eta_0}{4\pi}\frac{1}{(1+\sqrt{\varepsilon_{\rm r}})^2}. \tag{37}$$

Therefore, the enhancement $E_{\rm P}$ defined in Section III-C is

$$E_{\rm P} = \frac{4}{(1+\sqrt{\varepsilon_{\rm r}})^2} \tag{38}$$

which has its maximum value $E_{\rm P_{max}} = 4$ when $\varepsilon_{\rm r} = 0$. It can be noted that in this case the enhancement $E_{\rm P}$ has an upper limit, whereas in the case of the grounded plasma slab it can be made arbitrarily large by a proper choice of the physical and geometrical parameters [see (25)].

Turning now to the directivity at broadside, according to (9) this is given by

$$D = \frac{2\pi}{2(1+\sqrt{\varepsilon_{\rm r}})^2}\left[\int_0^{\theta_{\rm c}} \frac{\cos^2\theta}{(\cos\theta+\sqrt{\varepsilon_{\rm r}-\sin^2\theta})^2}{\rm d}\theta + \frac{1}{1-\varepsilon_{\rm r}}\int_{\theta_{\rm c}}^{\frac{\pi}{2}} \cos^2\theta\, e^{-2k_0 h_{\rm s}\sqrt{\sin^2\theta-\varepsilon_{\rm r}}}{\rm d}\theta\right]^{-1}. \tag{39}$$

For a fixed value of the normalized distance $\zeta_{\rm s} = k_0 h_{\rm s}$, D has a maximum for $\varepsilon_{\rm r} = 0$, as can be seen in Fig. 12(a), where different values of $\zeta_{\rm s}$ are considered. On the other hand, when $\varepsilon_{\rm r} = 0$, the first integral in (39) is zero and the second one can

be asymptotically evaluated for large values of $\zeta_{\rm s}$ by a simple integration by parts. The result is that $D \sim \pi\zeta_{\rm s}$, as can be verified in Fig. 12(b). When $\varepsilon_{\rm r} \neq 0$, the directivity increases with $\zeta_{\rm s}$ and tends to a limit value [see Fig. 12(b)]; however, such a limit value can be made arbitrarily large by choosing a sufficiently low value of $\varepsilon_{\rm r}$.

From the above results it can be concluded that, while the angular confinement of radiation close to broadside in the semi-infinite plasma problem can be related to a "lens" effect caused by the refraction process at the air-plasma interface, the significant enhancement of radiation at broadside is an intrinsically modal phenomenon related to the excitation of a leaky wave, and is thus only observed in the finite-thickness plasma-slab problem. Furthermore, a numerical calculation reveals that the directivity of the slab structure is much higher than that of the half-space structure, for the same distance of the source from the interface. Therefore, while a ray-optics effect plays a role in explaining the high directivity seen in the slab structure, the dominant physical mechanism is that of a leaky wave.

IV. Periodic Structures and Full-Wave Analysis

In this section, numerical results are presented for the radiation patterns of a line source embedded in a periodic metamaterial structure, in order to validate the analysis presented in the previous sections, which was based on a homogeneous grounded-slab model. In particular, full-wave simulations have been performed in order to determine the numerically-exact radiation pattern for the structure shown in Fig. 1(a), consisting of a line source inside a finite number of periodic layers of perfectly conducting cylinders.

The radiation patterns have been obtained by using the reciprocity theorem, which provides a convenient means to obtain the far-field pattern as it only involves a numerical solution of the structure under plane-wave incidence [45]. Reciprocity has also been used previously to obtain the far-field patterns of dipole sources in homogeneous layered media [46] and dipole sources in the presence of infinite periodic structures [47]. Although the metamaterial slab in Fig. 1(a) is not homogeneous, reciprocity still applies since the slab medium consists of only perfectly conducting cylinders above a ground plane, and perfect conductors are reciprocal objects. (As a side remark, it is interesting to note that reciprocity places restrictions on the spatially dispersive behavior of the metamaterial slab permittivity, as discussed in [48].)

In the reciprocity method for the structure considered here, a 1-Amp "testing" line source "b" is placed in the far field at (ρ, θ). The far field from the original line source "a" inside the metamaterial slab at $(0, h_{\rm s})$ [see Fig. 1(a)] is simply the reaction $\langle a, b\rangle$ [45]. (Because of the 1-D nature of the problem considered here, reaction actually denotes reaction per unit length in the y direction.) By reciprocity, this is the same as the reaction $\langle b, a\rangle$, which physically represents the electric field $E_y(0, h_{\rm s})$ at the location of the original line source, due to the incident field of the testing line source. Since the testing line source is in the far field, the incident field that it produces near the metamaterial slab is essentially a plane wave with an amplitude at the origin that is

$$E_0 = \frac{\mu_0}{4j}\sqrt{\frac{2}{\pi k_0}}e^{\frac{j\pi}{4}}\frac{e^{-jk_0\rho}}{\sqrt{\rho}} \tag{40}$$

Hence, the far-field pattern $E_y(\rho, \theta)$ is the same as the field $E_y(0, h_{\rm s})$ when the metamaterial slab is illuminated by an incident plane wave of amplitude E_0 arriving from the direction angle θ. This field is calculated by using a periodic moment method, so that the analysis domain can be restricted to a single spatial period (unit cell) of the structure. The electric field integral equation (EFIE) is enforced on the surface of the N cylinders within the unit cell, with N being the number of cylinder layers comprising the metamaterial slab. Sixteen pulse basis and testing functions have been adopted on each cylinder for the numerical solution. The periodic free-space Green's function that is used in the periodic moment-method solution has been accelerated using the Ewald method as described in [49], for improved computational efficiency.

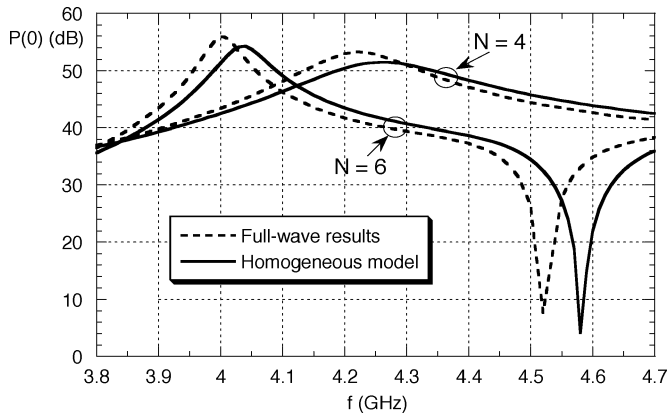

Fig. 13. Power density radiated at broadside versus frequency: comparisons between full-wave simulations and results obtained with the homogeneous grounded-slab model, for the structure in Fig. 1(a) with $N = 6$ and $N = 4$ layers of PEC cylinders. *Parameters*: $a = 0.5$ mm, $d = 20$ mm. *Parameters of the homogeneous model*: $h = Nd$, $f_{\rm p} = 3.8413$ GHz.

In Fig. 13, the power density at broadside is reported as a function of frequency for the metamaterial structure in Fig. 1(a), with parameters $a = 0.5$ mm and $d = 20$ mm, and with $N = 4$ and $N = 6$ layers of cylinders, respectively. Note that in Fig. 1 the bottom cylinder is centered $d/2$ above the ground plane and the source is located at a distance $z = Nd/2$ above the ground plane, i.e., in the middle of the structure. Full-wave results are compared here with those obtained from the corresponding homogeneous grounded slab model. The equivalent height h has been chosen equal to Nd, which takes into account the fringing fields at the top and bottom layers of the structure [12]. Therefore, the source is located at $h_{\rm s} = h/2$. Furthermore, an effective plasma frequency $f_{\rm p} = 3.8413$ GHz has been used, calculated according to the following approximate formula, valid in the limit of small cylinder radius with respect to the spatial period [50]

$$f_{\rm p} = \frac{c}{d}\frac{1}{\sqrt{2\pi\left(\ln\frac{d}{2\pi a} + 0.5275\right)}}. \tag{41}$$

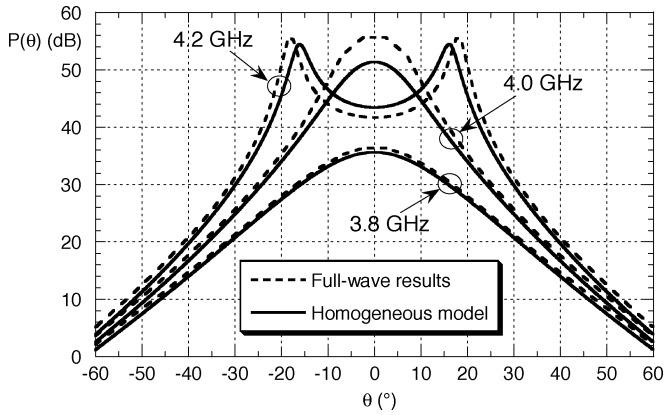

Fig. 14. Radiation patterns at three different frequencies: comparisons between full-wave simulations and results obtained with the homogeneous grounded-slab model, for the structure in Fig. 13, with $N = 6$ layers of PEC cylinders.

As can be seen, in both cases the behavior of the power density at broadside as a function of frequency is correctly predicted by the homogeneous model, thus confirming the effectiveness of this model in capturing the essential physical mechanisms of radiation for this class of structures, even in the presence of a small number of periodic layers. However, it may be noted that the optimum frequency obtained with the homogeneous model is shifted with respect to the one obtained from the full-wave simulations. This is probably due to the use of an approximate formula for the calculation of the effective plasma frequency of the homogenized medium, and to the adopted equivalent thickness for the homogeneous slab. With reference to the latter parameter, although it is shown in [12] that the choice $h = Nd$ is suitable for reproducing the plane-wave reflection and transmission features of a wire-medium slab in free space, it may well not be the optimal choice for describing modal propagation phenomena and radiation from finite sources in grounded wire-medium slabs.

In Fig. 14, radiation patterns are shown at three different frequencies for the same structure considered in Fig. 13 with $N = 6$ layers of cylinders. At $f = 3.8$ GHz the equivalent plasma is opaque, and a relatively broad beam pointing at broadside is radiated, with low values of the power density. At $f = 4$ GHz the plasma is transparent, the beam still points at broadside, and the level of radiated power density at broadside is maximum, so that the beam is on the verge of splitting. Finally, at $f = 4.2$ GHz two well separated peaks are visible, and the pointing angles are in very good agreement with those predicted by the homogeneous model, corresponding to the angles of leaky-wave radiation. Again, except for the above-mentioned frequency shift, the homogeneous model correctly reproduces the shape of the radiation pattern and its evolution with frequency.

V. Conclusion

In this paper radiation from a line source embedded in a plasma-like metamaterial slab over a ground plane has been studied. The extremely high directivity attainable with this kind of structure has been investigated by means of a simple model characterized by a frequency-dependent plasma-like permittivity.

Particular attention has been devoted to broadside radiation, deriving simple approximate formulas for the optimum slab thickness or frequency to maximize the radiated power density, for the directivity, and for the relevant pattern bandwidth of the antenna.

Furthermore, the fundamental mechanism of radiation responsible for the large power density at broadside and the high directivity has been shown here to be due to the excitation of a leaky wave supported by the structure. In particular, maximum power density radiated at broadside is obtained when the leaky mode has small and nearly equal values of the phase and attenuation constants. Directivity and bandwidth have also been expressed in terms of the attenuation constant of the leaky wave.

The case of a line source embedded within a semi-infinite plasma region has also been considered. In this case there is no leaky wave, and an increase in the directivity occurs only by virtue of a "ray-optics" effect, caused by the refraction of the waves at the interface. Although large directivities may be obtained with the plasma half-space structure (provided the source is sufficiently far from the interface), the power density at broadside may only be enhanced by a modest amount (at most a factor of 4).

Numerical results for actual metamaterials based on full-wave simulations of specific structures composed of a finite number of layers of circular conducting cylinders have been presented. These results validate the analysis based on a homogeneous slab model, and confirm the conclusions obtained from it.

Finally, we stress that the present 2-D investigation provides fundamental background information for the more involved 3-D problem of a wire-medium slab excited by an elemental dipole source. In fact, it can easily be seen by reciprocity that the shape of the H-plane radiation patterns of a dipole and of a line source parallel to the axis of the wires are exactly the same. On the other hand, the adopted isotropic plasma model is only suitable for treating 2-D propagation of TM_y polarized waves propagating in the xz plane, whereas the 3-D study requires taking into account the anisotropic and spatially-dispersive nature of the wire medium [51]. Nevertheless, the E-plane pattern from a dipole source can be shown to be approximately equal to the H-plane pattern of the same dipole source near the beam peak. Hence knowledge of the beam shape in both principal planes for the dipole source can be inferred from the H-plane pattern of the line source. A demonstration of this property, as well as other results for the 3-D problem, will be the subject of future work.

Acknowledgment

The authors would like to thank Prof. F. Mesa from the University of Seville for interesting discussions on the reciprocity method and the corresponding restrictions on the permittivity of the metamaterial slab.

REFERENCES

[1] E. Yablonovitch, "Photonic band-gap structures," *J. Opt. Soc. Amer. B*, vol. 10, pp. 283–294, Feb. 1993.

[2] J. D. Joannopoulos, R. D. Meade, and J. N. Winn, *Photonic Crystals. Molding the Flow of Light*. Princeton, NJ: Princeton Univ. Press, 1995.

[3] D. Sievenpiper, L. Zhang, R. F. J. Broas, N. G. Alexópoulos, and E. Yablonovitch, "High-impedance electromagnetic surfaces with a forbidden frequency band," *IEEE Trans. Microwave Theory Tech.*, vol. 47, pp. 2059–2074, Nov. 1999.

[4] W. M. Merrill, C. A. Kyriazidou, H. F. Contopanagos, and N. G. Alexópoulos, "Electromagnetic scattering from a PBG material excited by an electric line source," *IEEE Trans. Microwave Theory Tech.*, vol. 47, pp. 2105–2114, Nov. 1999.

[5] P. de Maagt, R. Gonzalo, Y. C. Vardaxoglou, and J.-M. Baracco, "Electromagnetic bandgap antennas and components for microwave and (sub)millimeter wave applications," *IEEE Trans. Antennas Propag.*, vol. 51, pp. 2667–2677, Oct. 2003.

[6] J. Brown, "Artificial dielectrics having refractive indices less than unity," *Proc. Inst. Elect. Eng.*, vol. 100, pp. 51–62, May 1953.

[7] R. N. Bracewell, "Analogues of an ionized medium: applications to the ionosphere," *Wireless Engr.*, vol. 31, pp. 320–326, Dec. 1954.

[8] W. Rotman, "Plasma simulation by artificial dielectrics and parallel-plate media," *IRE Trans. Antennas Propag.*, vol. AP-10, pp. 82–95, Jan. 1962.

[9] D. F. Sievenpiper, M. E. Sickmiller, and E. Yablonovitch, "3-D wire mesh photonic crystals," *Phys. Rev. Lett.*, vol. 76, pp. 2480–2483, 1996.

[10] J. B. Pendry, A. J. Holden, W. J. Stewart, and I. Youngs, "Extremely low frequency plasmons in metallic mesostructures," *Phys. Rev. Lett.*, vol. 76, pp. 4773–4776, 1996.

[11] D. Felbacq and G. Bouchitté, "Homogenization of a set of parallel fibers," *Waves in Random Media*, vol. 7, pp. 245–256, 1997.

[12] G. Guida, D. Maystre, G. Tayeb, and P. Vincent, "Mean-field theory of two-dimensional metallic photonic crystals," *J. Opt. Soc. Amer. B*, vol. 15, pp. 2308–2315, 1998.

[13] J. B. Pendry, A. J. Holden, D. J. Robbins, and W. J. Stewart, "Low frequency plasmons in thin-wire structures," *J. Phys. Condens. Matter*, vol. 10, pp. 4785–4809, 1998.

[14] D. R. Smith, D. C. Vier, W. Padilla, S. C. Nemat-Nasser, and S. Schultz, "Loop-wire medium for investigating plasmons at microwave frequencies," *Appl. Phys. Lett.*, vol. 75, pp. 1425–1427, 1999.

[15] J. B. Pendry, A. J. Holden, D. J. Robbins, and W. J. Stewart, "Magnetism from conductors and enhanced nonlinear phenomena," *IEEE Microwave Theory Tech.*, vol. 47, pp. 2075–2084, Nov. 1999.

[16] D. R. Smith, W. J. Padilla, D. C. Vier, S. C. Nemat-Nasser, and S. Schultz, "Composite medium with simultaneously negative permeability and permittivity," *Phys. Rev. Lett.*, vol. 84, pp. 4184–4187, 2000.

[17] R. A. Shelby, D. R. Smith, S. C. Nemat-Nasser, and S. Schultz, "Microwave transmission through a two-dimensional, isotropic, left-handed metamaterial," *Appl. Phys. Lett.*, vol. 78, pp. 489–491, 2001.

[18] J. B. Pendry, "Negative refraction makes a perfect lens," *Phys. Rev. Lett.*, vol. 85, pp. 3966–3969, Oct. 2000.

[19] L. Liu, C. Caloz, and T. Itoh, "Dominant mode (DM) leaky-wave antenna with backfire-to-endfire scanning capability," *Electron. Lett.*, vol. 38, pp. 1414–1416, Nov. 2000.

[20] N. Engheta, "An idea for thin subwavelength cavity resonators using metamaterials with negative permittivity and permeability," *IEEE Antennas Wireless Propag. Lett.*, vol. 1, pp. 10–13, 2002.

[21] I. V. Shadrivov, A. A. Sukhorukov, and Y. S. Kivshar, "Beam shaping by a periodic structure with negative refraction," *Appl. Phys. Lett.*, vol. 82, pp. 3820–3822, 2003.

[22] M. Antoniades and G. V. Eleftheriades, "Compact, linear, lead/lag metamaterial phase shifters for broadband applications," *IEEE Antennas Wireless Propag. Lett.*, vol. 2, pp. 103–106, Jul. 2003.

[23] C. Caloz and T. Itoh, "A novel mixed conventional microstrip and composite right/left-handed backward-wave directional coupler with broadband and tight coupling characteristics," *IEEE Microw. Wireless Compon. Lett.*, vol. 14, pp. 31–33, Jan. 2004.

[24] R. Islam and G. V. Eleftheriades, "Phase-agile branch-line couplers using metamaterial lines," *IEEE Microw. Wireless Compon. Lett.*, vol. 14, pp. 340–342, Jul. 2004.

[25] T. Itoh, "Invited paper: prospects for metamaterials," *Electron. Lett.*, vol. 40, pp. 972–973, Aug. 2004.

[26] K. C. Gupta, "Narrow-beam antennas using an artificial dielectric medium with permittivity less than unity," *Electron. Lett.*, vol. 7, pp. 16–18, Jan. 1971.

[27] G. Poilasne, P. Pouliguen, J. Lenormand, K. Mahdjoubi, C. Terret, and P. Gelin, "Theoretical study of interactions between antennas and metallic photonic bandgap materials," *Microwave Opt. Technol. Lett.*, vol. 15, pp. 384–389, Mar. 1997.

[28] A. Fehrembach, S. Enoch, and A. Sentenac, "Highly directive light sources using two-dimensional photonic crystal slabs," *Appl. Phys. Lett.*, vol. 79, pp. 4280–4282, Dec. 2001.

[29] J. S. Foresi, P. R. Villeneuve, J. Ferrera, E. R. Thoen, G. Steinmeyer, S. Fan, J. D. Joannopoulos, L. C. Kimerling, H. I. Smith, and E. P. Ipeen, "Photonic bandgap microcavities in optical waveguides," *Nature*, vol. 390, pp. 143–145, 1997.

[30] M. Thèvenot, C. Cheype, A. Reineix, and B. Jecko, "Directive photonic bandgap antennas," *IEEE Trans. Microwave Theory Tech.*, vol. 47, pp. 2115–2122, Nov. 1999.

[31] C. Cheype, C. Serier, M. Thèvenot, T. Monédière, A. Reineix, and B. Jecko, "An electromagnetic bandgap resonator antenna," *IEEE Trans. Antennas Propag.*, vol. 50, pp. 1285–1290, Sep. 2002.

[32] B. Temelkuaran, M. Bayindir, E. Ozbay, R. Biswas, M. M. Sigalas, G. Tuttle, and K. M. Ho, "Photonic crystal-based resonant antenna with a very high directivity," *J. Appl. Phys.*, vol. 87, pp. 603–605, 2000.

[33] S. Enoch, G. Tayeb, P. Sabouroux, N. Guérin, and P. Vincent, "A metamaterial for directive emission," *Phys. Rev. Lett.*, vol. 89, pp. 213 902-1–213 902-4, Nov. 2002.

[34] H. Boutayeb, K. Mahdjoubi, and A. C. Tarot, "Design of a directive and matched antenna with a planar EBG structure," in *IEEE AP-S Int. Symp. Digest* , Monterey, CA, Jun. 20–25, 2004, pp. 835–838.

[35] T. Tamir and A. A. Oliner, "The influence of complex waves on the radiation field of a slot-excited plasma layer," *IRE Trans. Antennas Propag.*, vol. AP-10, pp. 55–65, Jan. 1962.

[36] ——, "The spectrum of electromagnetic waves guided by a plasma layer," *Proc. IEEE*, vol. 51, pp. 317–332, Feb. 1963.

[37] P. Baccarelli, P. Burghignoli, F. Frezza, A. Galli, P. Lampariello, G. Lovat, and S. Paulotto, "Effects of leaky-wave propagation in metamaterial grounded slabs excited by a dipole source," *IEEE Trans. Microwave Theory Tech.*, vol. 53, pp. 32–44, Jan. 2005.

[38] I. J. Bahl and K. C. Gupta, "A leaky-wave antenna using an artificial dielectric medium," *IEEE Trans. Antennas Propag.*, vol. AP-22, pp. 119–122, Jan. 1974.

[39] ——, "Frequency scanning by leaky-wave antennas using artificial dielectrics," *IEEE Trans. Antennas Propag.*, vol. AP-23, pp. 584–589, Apr. 1975.

[40] H.-Y. D. Yang, N. G. Alexópoulos, and E. Yablonovitch, "Photonic band-gap materials for high-gain printed circuit antennas," *IEEE Trans. Antennas Propag.*, vol. 45, pp. 185–187, Jan. 1997.

[41] R. E. Collin, *Field Theory of Guided Waves*, 2nd ed. Piscataway, NJ: IEEE Press, 1991.

[42] L. B. Felsen and N. Marcuvitz, *Radiation and Scattering of Waves*. Piscataway, NJ: IEEE Press, 1994.

[43] T. Tamir and A. A. Oliner, "Guided complex waves. Part I: fields at an interface. Part II: relation to radiation patterns," *Proc. Inst. Elect. Eng.*, vol. 110, pp. 310–334, Feb. 1963.

[44] S. Wolfram. (2005) The Mathematica Homepage. [Online]. Available: http://www.wolfram.com

[45] R. F. Harrington, *Time-Harmonic Electromagnetic Fields*. Piscataway, NJ: IEEE Press, 2001.

[46] D. R. Jackson and N. G. Alexópoulos, "Gain enhancement methods for printed circuit antennas," *IEEE Trans. Antennas Propag.*, vol. 33, pp. 976–987, Sep. 1985.

[47] T. Zhao, D. R. Jackson, J. T. Williams, H. Y. Yang, and A. A. Oliner, "2-D periodic leaky-wave antennas—part I: metal patch design," *IEEE Trans. Antennas Propag.*, vol. 53, pp. 3505–3514, Nov. 2005.

[48] P. R. McIsaac, "A general reciprocity theorem," *IEEE Trans. Microwave Theory Tech.*, vol. 27, pp. 340–342, April 1979.

[49] F. Capolino, D. R. Wilton, and W. A. Johnson, "Efficient calculation of the 2-D Green's function for 1-D periodic structures using the Ewald method," *IEEE Trans. Antennas Propag.*, vol. 53, pp. 2977–2984, Sep. 2005.

[50] P. A. Belov, S. A. Tretyakov, and A. J. Viitanen, "Dispersion and reflection properties of artificial media formed by regular lattices of ideally conducting wires," *J. Electromag. Waves Appl.*, vol. 16, no. 8, pp. 1153–1170, Sep. 2002.

[51] P. A. Belov, R. Marqués, S. I. Maslovski, M. Silveirinha, C. R. Simovski, and S. A. Tretyakov, "Strong spatial dispersion in wire media in the very large wavelength limit," *Phys. Rev. B*, vol. 67, pp. 113 103-1–113 103-4, 2003.

Giampiero Lovat (S'02–M'06) was born in Rome, Italy, on May 31, 1975. He received the Laurea degree (*cum laude*) in electronic engineering and the Ph.D. degree in applied electromagnetics, both from "La Sapienza" University of Rome, Rome, Italy, in 2001 and 2004, respectively.

From January 2004 to July 2004, he was a Visiting Scholar at the University of Houston, Houston, Texas. In 2005, he joined the Electrical Engineering Department of "La Sapienza" University of Rome, where he is currently an Associate Researcher. His scientific interests include theoretical and numerical studies on leakage phenomena in planar structures, guidance and radiation in metamaterials, general periodic structures, and EMC.

Dr. Lovat received a Young Scientist Award from the 2005 URSI General Assembly, New Delhi, India.

Paolo Burghignoli (S'97–M'01) was born in Rome, Italy, on February 18, 1973. He received the Laurea degree (*cum laude*) in electronic engineering and the Ph.D. degree in applied electromagnetics, both from "La Sapienza" University of Rome, Rome, Italy, in 1997 and 2001, respectively.

In 1997, he joined the Electronic Engineering Department of "La Sapienza" University of Rome, where he is currently an Associate. From January 2004 to July 2004, he was a Visiting Research Assistant Professor at the University of Houston, Houston, Texas. His scientific interests include analysis and design of planar leaky-wave antennas, numerical methods for the analysis of passive guiding and radiating microwave structures, periodic structures, and propagation and radiation in metamaterials.

Dr. Burghignoli received the Graduate Fellowship Award from IEEE Microwave Theory and Techniques Society in 2003, and the Raj Mittra Travel Grant for Junior Researchers from the 2005 Antennas and Propagation Symposium, Washington, DC.

Filippo Capolino (S'94–M'97–SM'04) was born in Florence, Italy, in 1967. He received the Laurea degree (*cum laude*) in electronic engineering and the Ph.D. degree, from the University of Florence, Italy, in 1993 and 1997, respectively.

From 1994 to 2000, he was a lecturer of antennas at the Diploma di Laurea, University of Siena, Italy, where he has been a Research Associate until 2002 and presently employed as an Assistant Professor. From 1997 to 1998, he was a Fulbright Research Visitor with the Department of Aerospace and Mechanical Engineering, Boston University, Boston, MA, where he continued his research with a Grant from the Italian National Council for Research (CNR), from 1998 to 1999. From 2000 to 2001, he was a Research Assistant Visiting Professor with the Department of Electrical and Computer Engineering, University of Houston, Houston, TX, where he is now an Adjunct Assistant Professor. In November and December 2003, he was an Invited Assistant Professor at the Institut Fresnel, Marseille, France, working on EBG antennas. His research interests include theoretical and applied electromagnetics focused on high-frequency, short-pulse radiation, array antennas, periodic structures, numerical modeling, and metamaterials. He is the coordinator of the Siena Unit for the Network of Excellence "Metamorphose" on Metamaterials of the sixth framework program of the European Union.

Dr. Capolino was awarded with a MMET'94 Student Paper Competition Award in 1994, the Raj Mittra Travel Grant for Young Scientists in 1996, the "Barzilai" prize for the best paper at the National Italian Congress of Electromagnetism (XI RiNEm) in 1996, and a Young Scientist Award for participating at the URSI Int. Symp. Electromagn. Theory in 1998. He received the R.W. P. King Prize Paper Award from the IEEE Antennas and Propagation Society for the Best Paper of the Year 2000, by an author under 36. He is an Associate Editor for the IEEE TRANSACTIONS ON ANTENNAS AND PROPAGATION.

David R. Jackson (S'83–M'84–SM'95–F'99) was born in St. Louis, MO, on March 28, 1957. He received the B.S.E.E. and M.S.E.E. degrees from the University of Missouri, Columbia, in 1979 and 1981, respectively, and the Ph.D. degree in electrical engineering from the University of California, Los Angeles, in 1985.

From 1985 to 1991, he was an Assistant Professor in the Department of Electrical and Computer Engineering at the University of Houston, Houston, TX, where from 1991 to 1998, he was an Associate Professor, and since 1998 he has been a Professor. He has served as an Associate Editor for the journal of *Radio Science*, the *International Journal of RF*, and *Microwave Computer-Aided Engineering*. His present research interests include microstrip antennas and circuits, leaky-wave antennas, leakage and radiation effects in microwave integrated circuits, periodic structures, and EMC.

Dr. Jackson is presently serving as the Chair for the International Union of Radio Science (URSI) U.S. Commission B and the Chair of the Transnational Committee of the IEEE AP Society. He is also on the Editorial Board for the IEEE TRANSACTIONS ON MICROWAVE THEORY AND TECHNIQUES. Previously, he has been the Chapter Activities Coordinator for the IEEE AP Society, a Distinguished Lecturer for the AP Society, an Associate Editor for the IEEE TRANSACTIONS ON ANTENNAS AND PROPAGATION, and a member of the AdCom for the AP Society.

Donald R. Wilton (S'63–M'65–SM'80–F'87) was born in Lawton, OK, on October 25, 1942. He received the B.S., M.S., and Ph.D. degrees from the University of Illinois, Urbana-Champaign, in 1964, 1966, and 1970, respectively.

From 1965 to 1968 he was with Hughes Aircraft Co., Fullerton, CA, engaged in the analysis and design of phased array antennas. From 1970 to 1983 he was with the Department of Electrical Engineering, University of Mississippi, and since 1983 he has been Professor of Electrical Engineering at the University of Houston. From 1978 to 1979 he was a Visiting Professor at Syracuse University. During 2004 and 2005 he was a Visiting Scholar at the Polytechnic of Turin, Italy, the Sandia National Laboratories, and the University of Washington. His primary research interest is in computational electromagnetics, and he has published, lectured, and consulted extensively in this area.

Dr. Wilton is a member of Commission B of URSI, in which he has held various offices including Chair of U. S. Commission B. He received the IEEE Third Millenium Medal. He has served the IEEE Antennas and Propagation Society as an Associate Editor of the TRANSACTIONS ON ANTENNAS AND PROPAGATION, as a Distinguished National Lecturer, and as a member of AdCom.